Spectroscopic and Kinetic Properties of HO_2 Radicals and the Enhancement of the HO_2 Self Reaction by CH_3OH and H_2O

Yongxin Tang, Geoffrey S. Tyndall,* and John J. Orlando

Atmospheric Chemistry Division, National Center for Atmospheric Research, Boulder, Colorado 80307

Received: June 4, 2009; Revised Manuscript Received: November 18, 2009

The line center absorption cross sections and the rate constants for self-reaction of hydroperoxy radicals (HO_2) have been examined in the temperature range of 253−323 K using pulsed laser photolysis combined with tunable diode laser absorption in the near-IR region. The transition probed was in the $2\nu_1$ OH overtone transition at 1506.43 nm. The temperature dependence of the rate constant (k) for the $HO_2 + HO_2$ reaction was measured relative to the recommended value at 296 K, giving $k = (3.95 \pm 0.45) \times 10^{-13} \times \exp[(439 \pm 39)/T]$ cm^3 molecule^{-1} s^{-1} at a total pressure of 30 Torr ($N_2 + O_2$). After normalizing our determination and previous studies at low pressure, we recommend $k = (2.45 \pm 0.50) \times 10^{-13} \times \exp[(565 \pm 130)/T]$ cm^3 molecule^{-1} s^{-1} ($0 < P < 30$ Torr, 95% confidence limits). The observed rate coefficient, k_{obs}, increases linearly with CH_3OH concentration, and the enhancement coefficient (k'), defined by $k_{obs} = k + k'[CH_3OH]$, is found to be $(3.90 \pm 1.87) \times 10^{-35} \times \exp[(3849 \pm 135)/T]$ cm^6 molecule^{-2} s^{-1} at 30 Torr. The analogous water vapor enhancement coefficient (k'') is $(1.16 \pm 0.58) \times 10^{-36} \times \exp[(4614 \pm 145)/T]$ cm^6 molecule^{-2} s^{-1}. The pressure-broadened HO_2 absorption cross section is independent of temperature in the range studied. The line center absorption cross sections at 1506.43 nm, after correction for instrumental broadening, are $(4.3 \pm 1.1) \times 10^{-19}$, $(2.8 \pm 0.7) \times 10^{-19}$, and $(2.0 \pm 0.5) \times 10^{-19}$ cm^2/molecule at total pressures of 0, 30, and 60 Torr, respectively (95% confidence limits).

Introduction

Hydroperoxy (HO_2) radicals play important roles in both the troposphere and the stratosphere. In the troposphere, HO_2 radicals are central to the production of ozone and the generation of hydroxyl radicals. In the stratosphere, they are involved in catalytic cycles which destroy ozone. One of the major removal mechanisms for hydroperoxy radicals is the combination reaction, which can be represented by reactions 1 and 2.

$$HO_2 + HO_2 \rightarrow O_2 + H_2O_2 \quad (1)$$

$$HO_2 + HO_2 + M \rightarrow O_2 + H_2O_2 + M \quad (2)$$

The kinetics of reactions 1 and 2 has been extensively studied. The reaction, as we presently understand it, has a bimolecular term and a pressure-dependent term. Both terms have negative temperature dependences, but the temperature dependence of the reaction is still somewhat uncertain. Atkinson et al.[1] and Wallington et al.[2] evaluated previous studies and recommended the results derived by Kircher and Sander[3]

$$k = k_1 + k_2 = 2.2 \times 10^{-13} \times \exp(600/T) + 1.9 \times 10^{-33} \times [M] \times \exp(980/T) \quad (3)$$

where the first term is the rate constant for the bimolecular reaction channel, reaction 1, at zero pressure. The second term is the rate constant for the termolecular reaction channel, reaction 2, which makes the total rate constant pressure-dependent.

It has been shown that the presence of H_2O, NH_3, and CH_3OH[4−10] enhances the rate constant of the $HO_2 + HO_2$ reaction through complexation with HO_2. Water vapor has a significant effect on the environmental chemistry of HO_2 radicals by increasing its loss rate in the lower troposphere. While not atmospherically important, the effect of CH_3OH on the HO_2 decay rate constant also has to be quantified since CH_3OH is frequently used as a precursor for HO_2 radicals in laboratory studies. Christensen and coauthors[6] studied the complexation between CH_3OH and HO_2 and noted that Kircher et al.[3] had not accounted for the CH_3OH enhancement effect on the HO_2 decay rate constant at low temperature. In contrast to previous studies, Christensen et al. measured a weak temperature dependence at 100 Torr.

$$k = 8.8 \times 10^{-13} \times \exp(210/T) \quad (4)$$

Christensen et al. suggested that their measurements improved the agreement of atmospheric models with measured profiles of H_2O_2 when compared to older measurements of the reaction rate. The latest Jet Propulsion Laboratory evaluation[11] included the results from Christensen et al. and recommended an intermediate activation energy

$$k = k_1 + k_2 = 3.5 \times 10^{-13} \times \exp(430/T) + 1.7 \times 10^{-33} \times [M] \times \exp(1000/T) \quad (5)$$

Most of the earlier studies used UV absorption near 220 nm to detect HO_2. Detection of peroxy radicals using UV absorption suffers from the disadvantage that the spectra are broad and unstructured. Kinetic studies of HO_2 in the presence of H_2O have to account for the presence of an absorbing product, H_2O_2, and potentially for absorption by the complex HO_2-H_2O. It is normally assumed that the complex formed has an identical absorption spectrum to that of uncomplexed HO_2.[2,11] On the other hand, the HO_2 absorption spectra in the near-IR are more structured, and thus, spectral interferences from other species are less likely than in the UV−vis region.[12−14] We have used absorption in the OH overtone band of HO_2 in the near-IR region

* To whom correspondence should be addressed. E-mail: tyndall@ucar.edu. Tel: 303-497-1472. Fax: 303-497-1400.

10.1021/jp905279b
Published on Web 12/16/2009

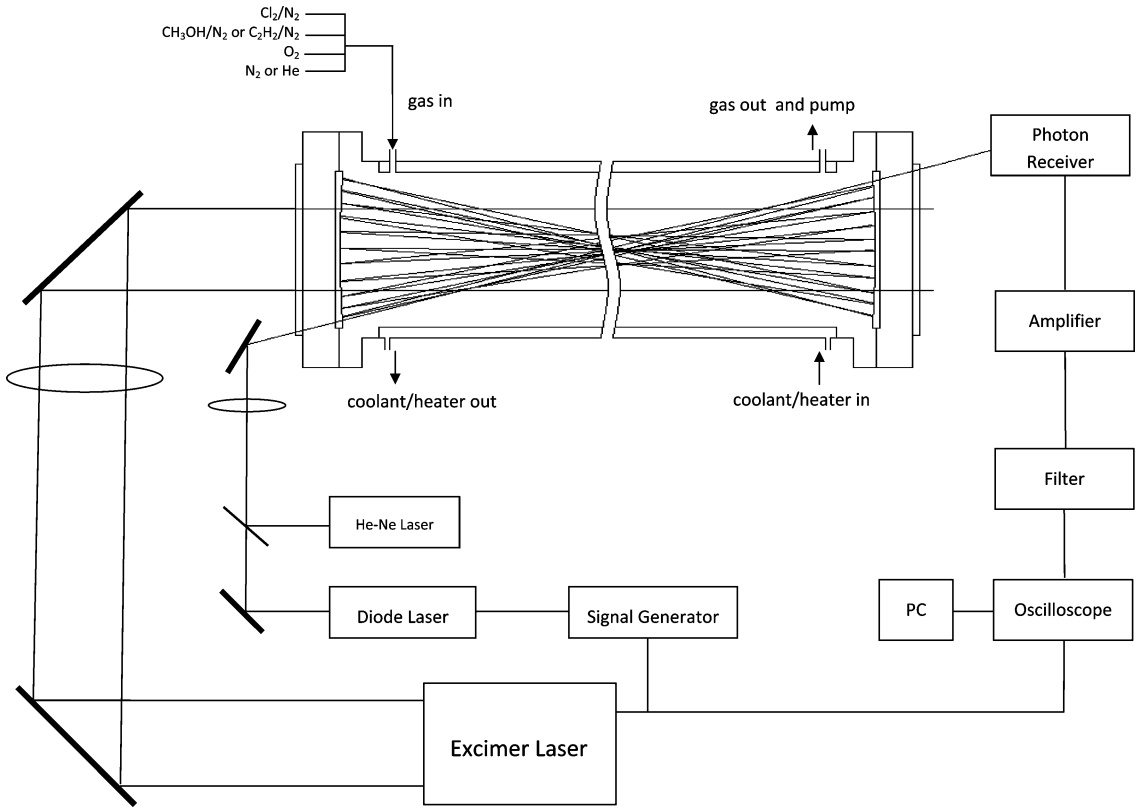

Figure 1. Schematic of the experimental setup. Only some of the 31 passes of the diode laser beam are depicted.

to measure the spectroscopic and kinetic properties of HO_2 radicals. However, there is a large uncertainty among the IR line center absorption cross sections of HO_2 radicals reported in the literature. For example, the absorption cross section at 1509.26 nm was reported to be 2.5×10^{-19} cm^2/molecule in 50 Torr of He by Thiebaud and coauthors in 2006,[12] while it was revised to 1.68×10^{-19} cm^2/molecule by the same group in 2007.[13] In an early study, Johnson et al.[14] gave an absorption cross section of 1.0×10^{-19} cm^2/molecule at this same wavelength. This was reported as Doppler-limited but was actually at 60 Torr (J. P. Burrows, personal communication, 2009).

We have examined the near-IR absorption cross sections of HO_2 radicals as a function of temperature, wavelength, and total pressure using flash photolysis combined with tunable diode laser detection. Using the measured absorption cross sections and the literature value of k at 298 K and 30 Torr, we studied the temperature-dependent rate constants of the HO_2 self-reaction along with the CH_3OH and water vapor enhancement coefficients between 253 and 323 K. The results are discussed in the following order, (1) HO_2 absorption spectrum and kinetic decays at 296 K, (2) determination of HO_2 absorption cross section relative to that of C_2H_2, (3) kinetics of HO_2 as a function of temperature, (4) pressure broadening of HO_2 spectral features and (5) effect of water vapor on the HO_2 spectrum and kinetics.

Experimental Section

The schematic of the experimental setup is shown in Figure 1. The flash photolysis experiments were conducted in an aluminum Herriott type cell, which was built based on the principles demonstrated by Pilgrim et al.[15] and Qian et al.[16] The overall length of the cell was approximately 103 cm, and the inner diameter of the main part of the cell was approximately 5.7 cm. The cell was sealed by a pair of CaF_2 windows, which were enclosed in a housing at room temperature and attached to the temperature-controlled flow cell by flanges. The temperature of the cell was controlled by a liquid ethanol bath (Neslab, ULT-80DD) or a water bath (Neslab, RTE-110). Thermocouples could be inserted into the gas flow to measure the temperature directly. The temperature of the gas was found to be constant to within ±2 K, and no significant gradients were measured along the length of the cell. During experiments, the thermocouples were withdrawn from the main gas flow and used to monitor temperature stability at the edge of the flow area (so as not to interfere with the optical measurements).

To generate HO_2, radiation from a XeF excimer laser (Lambda Physik, Compex 102) at 351 nm was introduced into the cell to photolyze Cl_2 in the presence of CH_3OH and O_2

$$Cl_2 \rightarrow 2Cl \qquad (\lambda = 351 \text{ nm}) \tag{6}$$

$$Cl + CH_3OH \rightarrow CH_2OH + HCl \tag{7}$$

$$CH_2OH + O_2 \rightarrow HO_2 + HCHO \tag{8}$$

Concentrations of the chemical species at room temperature were in the ranges of Cl_2: $\sim 1.8 \times 10^{15} - 4.4 \times 10^{15}$ molecule/cm^3, CH_3OH: $\sim 4.0 \times 10^{15} - 5.6 \times 10^{16}$ molecule/cm^3, and O_2: $\sim 2.2 \times 10^{17} - 4.4 \times 10^{17}$ molecule/cm^3. The buffer gas used in this work was mainly N_2. The excimer laser beam was rectangular in cross section and roughly 4 cm wide and 2 cm high as it passed through the cell. Excimer laser energies of 100 mJ/pulse were used, which led to pulse energies of 50−60 mJ at the reaction cell. A tunable diode laser (New Focus, TLB6326 Velocity) was used to probe HO_2 vibrational overtone absorption in the near-IR region. The extra cavity laser was continuously tunable from 1470 to 1545 nm, with a quoted line width of $<10^{-5}$ cm^{-1}. The output was typically 7 mW in single mode operation. The wavelength could be modulated by scanning the external grating using a piezoelectric drive. The probe laser

beam was reflected back and forth through the cell by two high-reflectance gold-coated mirrors (Rocky Mountain Instrument Co, Lafayette, CO). These mirrors were concave spherical with an identical radius of curvature of 50 cm, and each one was mounted in the housing by three adjustable screws. The gold coating covered ~1 cm of the outer circumference of the mirrors, except for a 25° gap on each mirror, which allowed the IR beam to enter and exit the cell. The distance between the mirrors was approximately 95 cm. The probe laser beam passed 31 times through the cell, which is partially depicted in Figure 1, before it left the cell from the rear end, where it was detected by an IR photon receiver (New Focus, Nirvana 2017). The input angle of the probe laser relative to the rear mirror was set to 168° to improve the overlap of the photolysis and probe laser beams. A collinear He−Ne laser beam was used to align the diode laser beam. The output signal was treated by a homemade battery-powered preamplifier (×22) and a low-frequency pass filter (HP, 5489A, in this work a 3 or 10 kHz threshold was employed) before being averaged and recorded by a digital oscilloscope (Lecroy, model 9450) and a computer. When operated at the 3 kHz bandwidth, the filter introduced some instrumental broadening of the absorption feature. This was accounted for by making measurements of the heights and the widths of the C_2H_2 and N_2O absorption lines in the same wavelength region with and without the filter. No absorption features due to methanol were observed in the spectral region used.

The oscilloscope was synchronously triggered by an electronic output from the excimer laser. A signal generator (Stanford Research Systems, DS345) was also triggered by the excimer laser and was used to drive the output of the diode laser. The diode laser was operated in burst scan mode and swept repeatedly through the absorption peak of interest, synchronized to the excimer pulse. Typically, the repetition rate of the excimer laser was 1 Hz, and the diode laser was scanned at 200 Hz in triangular trigger mode; therefore, spectra were recorded at 400 Hz in total for each excimer laser pulse. The HO_2 absorption spectra usually began at ~3 ms after the excimer laser pulse and ended at ~30−80 ms based on the HO_2 absorption intensity.

Methanol (Mallinckrodt, ChromAR HPLC) was purified by repeated freeze−pump−thaw processes before its vapor was diluted to 5−10% mixtures in nitrogen. Actual concentrations of the CH_3OH mixtures from the bulb were checked by using FTIR and found to agree within 10% with the measured pressure. Chlorine (U.S. Welding, G2.5) and acetylene (Airgas, atomic absorption grade) were diluted to 4−10% and to 0.009−3%, respectively, in N_2 without any further purification. N_2, O_2, and He (ultrahigh purity) were purchased from U.S. Welding. A small flow of N_2 was introduced through a glass bubbler filled with liquid water (Fisher, HPLC grade) to generate a flow of water vapor. All of the gas flows were adjusted by calibrated mass flow controllers (MKS Instruments, 1179A) with different scales (0−10, 0−100, or 0−1000 sccm). Typical total flow rates were between 110 and 440 sccm when the total pressure in the cell was smaller than 60 Torr, which led to a residence time smaller than 1 min (in most cases, ~26 s). The pressure in the photolysis cell was measured by Baratron capacitance manometers (MKS Instruments, 627B).

Results and Discussion

1. HO_2 Absorption Spectrum and HO_2 Self-Reaction. Hydroperoxy (HO_2) radicals were formed by the 351 nm XeF laser photolysis of Cl_2 in the presence of CH_3OH and O_2, reactions 6−8 above. HO_2 radicals have a structured O−H stretching overtone absorption in the near-IR region. In the wavelength region that we observed, the strongest HO_2 absorption peak lies at 1506.43 nm (~6638.20 cm^{-1}).[13] A typical series of scans through this line at a total pressure of 30 Torr is indicated in Figure 2a. The x axis is the time delay after the photolysis laser pulse. Each sweep of the diode laser takes 2.5 ms. There are 20 scans shown in the figure, which represents the HO_2 decay from ~3 to 50 ms. There is also another weaker HO_2 absorption peak on the edge of each scan, whose position is approximately 1506.45 nm (~6638.11 cm^{-1}). This weaker peak appears as a doublet since the diode laser begins to sweep back immediately after passing through it.

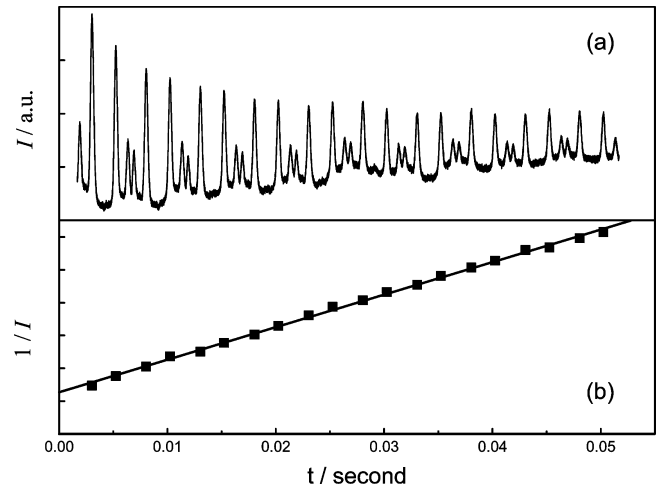

Figure 2. (a) Temporal behavior of the HO_2 absorption spectrum near 1506.43 nm (average over 10 excimer pulses). The excimer laser fires at $t = 0$ ms to produce HO_2. The diode laser is swept repetitively every 2.5 ms. The weaker peak is at a slightly higher frequency and appears doubled because of the timing of the reversal of the laser sweep. (b) The reciprocal of the HO_2 peak intensity as a function of time delay after the photolysis laser pulse. The linear least-squares fit gives a slope proportional to $2k_{obs}/(\sigma_{HO_2} \times L)$.

Shown in Figure 2b is a plot of the reciprocal of the corresponding HO_2 peak intensity as a function of the time delay along with a linear least-squares fit. The observed decay of HO_2 radicals due to the self-reaction (k_{obs}) obeys second-order kinetics, according to the following equation

$$\frac{1}{[HO_2]_t} - \frac{1}{[HO_2]_0} = 2 \times k_{obs} \times t \qquad (9)$$

where $[HO_2]_t$ and $[HO_2]_0$ are HO_2 concentrations at times equal to t and 0 after the photolysis laser pulse, respectively. The absorption of HO_2 obeys Beer's law

$$-\ln\left(1 - \frac{I}{I_0}\right) = \sigma_{HO_2} \times L_{total} \times [HO_2] \qquad (10)$$

where I_0 is the probe laser intensity without HO_2 absorption, I is the differential HO_2 absorption peak intensity, σ_{HO_2} is the HO_2 absorption cross section at the wavelength observed, and L_{total} is the total effective path length of photolysis/probe laser overlap. If L is defined as the mean single-pass overlap path length in cm, then L_{total} is equal to $L \times 31$. Normally, I/I_0 is small, <0.01, and eq 10 can be rearranged to

$$\frac{I}{I_0} = \sigma_{HO_2} \times L_{total} \times [HO_2] \qquad (11)$$

In practice, plots of I versus t were analyzed using a nonlinear fit of eq 9 rather than a linear fit of $1/[HO_2]$ versus t.

2. Determination of σ_{HO_2} and L at 60 Torr. As mentioned earlier, there is some disagreement among measurements of the HO_2 near-IR absorption cross sections. To aid in quantifying HO_2 concentrations, we undertook measurements of line center cross sections at a number of wavelengths. Although the Herriott multiple-pass cell has been widely used to measure weak absorptions, it is still not straightforward to determine the effective path length corresponding to the overlap of the photolysis and analysis beams. In this section, we determined σ_{HO_2} by comparing the absorption of HO_2 with that of acetylene (C_2H_2), and we use this information along with the accepted HO_2 self-reaction rate constant at 298 K and low pressure to determine the value of L.

The Cl atom concentration was measured by following the change in C_2H_2 concentration in the photolysis of $Cl_2/C_2H_2/O_2/N_2$ mixtures. The C_2H_2 absorption cross sections were measured separately in flowing mixtures using the full geometrical path length of the cell (31 m). The cross section at 1518.21 nm was $(3.7 \pm 0.2) \times 10^{-19}$ cm^2/molecule at a pressure of 60 Torr (O_2 and N_2 mixture). Back-to-back experiments were performed in which either HO_2 production or the loss of C_2H_2 was measured in order to derive the relative cross sections.

$$Cl + C_2H_2 + M \rightarrow ClC_2H_2 + M \quad (12)$$

$$ClC_2H_2 + O_2 \rightarrow HO_2 + CO + HC(O)Cl \quad (13a)$$

$$ClC_2H_2 + O_2 \rightarrow Cl + HC(O)CHO \quad (13b)$$

$$Cl + HC(O)CHO \rightarrow HCl + HC(O)CO \quad (14)$$

Thus, only changes in C_2H_2 occurring in the overlap volume of the two lasers were detected. The contents of the cell were irradiated by the excimer laser at the repetition rate of ~0.03 Hz, so that the gas mixture in the cell was replaced completely between excimer laser pulses. If the Cl_2 concentration and the excimer laser fluence remained constant, then the amount of HO_2 formed in the flash photolysis of a $Cl_2/CH_3OH/O_2/N_2$ mixture was equal to the amount of C_2H_2 lost in the photolysis of a $Cl_2/C_2H_2/O_2/N_2$ mixture. Hence, the absorption of the HO_2 produced can be equated to that of the C_2H_2 reacted using Beer's law

$$\sigma_{HO_2} = \frac{C_1}{C_2} \times \frac{Abs_{HO_2, t=3\,ms}}{\Delta Abs_{C_2H_2, t=10\,ms}} \times \sigma_{C_2H_2} \quad (15)$$

where $Abs_{HO_2, t=3\,ms}$ is the absorbance of HO_2 radicals generated from $Cl_2/CH_3OH/O_2$ photolysis reactions at the time delay of ~3 ms. $\Delta Abs_{C_2H_2, t=10\,ms}$ is the change in the C_2H_2 absorbances at ~10 ms after excimer laser photolysis of a $Cl_2/C_2H_2/O_2$ mixture. The reaction between C_2H_2 and Cl is relatively slow, but by working at 60 Torr, the rate coefficient is increased, and 90% of the Cl atoms are consumed inside of 3 ms. The constants C_1 and C_2 were obtained via simulation of the chemistry, conducted with the ACUCHEM program.[17] The mechanism included reactions of Cl atoms with C_2H_2 and HO_2 and the reactive channels for the reactions of O_2 with the $Cl-C_2H_2$ adduct shown above. The branching ratio k_{13a}/k_{13b} was set to 4:1. C_1 was used to extrapolate the measured HO_2 absorbance at 3 ms to that at zero time, while C_2 was used to relate the change in C_2H_2 to the actual Cl concentration because a fraction of Cl atoms reacts with glyoxal in reaction 14. Both constants were >0.8. Varying the branching ratio k_{13a}/k_{13b} in the range of 0.25−4.0 changed the value of C_2 by <20%. It should be noted that both constants change with the Cl concentration, but the ratio of C_1/C_2 is almost constant. For example, C_1/C_2 decreases less than 1% if the Cl concentration is doubled.

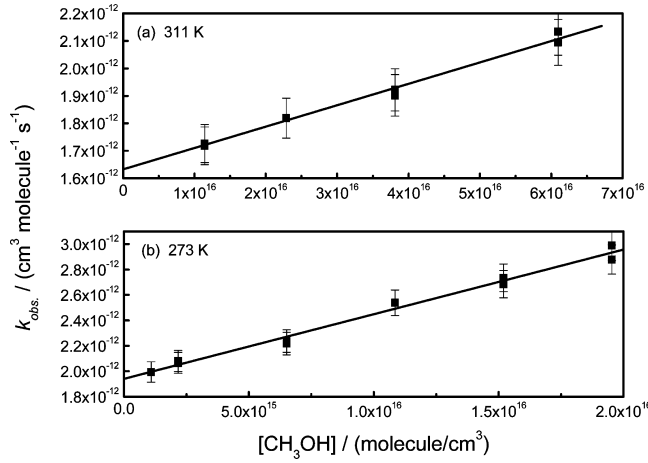

Figure 3. Observed total rate constants (k_{obs}) of the HO_2 self-reaction as a function of methanol concentration at different temperatures. The solid squares are measurements, and the straight lines are linear least-squares fits. The intercept is the rate constant of the HO_2 self-reaction at zero CH_3OH concentration (k), and the slope gives the CH_3OH enhancement coefficient (k').

The C_2H_2 concentration employed was $(5-7) \times 10^{13}$ molecule/cm^3, which was 3−4 times the initial Cl concentration. By using eq 15, we found σ_{HO_2} at a total pressure of 60 Torr (mainly N_2 and O_2) to be equal to 1.45×10^{-19} cm^2/molecule (further correction will be given in subsection 4) at both 296 and 263 K. An important result here is that σ_{HO_2} does not change appreciably with temperature. To check this, we directly compared the HO_2 peak intensities extrapolated to $t = 0$ from decays measured at different temperatures (296 and 253 K). After correcting for the excimer laser fluence and the Cl_2 density, the initial HO_2 intensities at 296 and 253 K varied by less than 5%. This also suggests that σ_{HO_2} does not change with temperature. The total uncertainty of σ_{HO_2} at 296 K is approximately 25% at the 95% confidence level, which includes the experimental uncertainties associated with the determination of the HO_2 absorbance (4%), the C_2H_2 absorption cross section (3%), and the C_2H_2 absorption change (9%), along with a 5% uncertainty associated with the modeling of the factor C_2. The total experimental uncertainty of σ_{HO_2} at 263 K is approximately 30%.

We use the value of σ_{HO_2} just determined and the accepted rate constant for HO_2 self-reaction at 298 K and low pressure to determine L. At 296 K, the CH_3OH enhancement effect on the rate constant of HO_2 decay is very small at low CH_3OH concentration. Adopting the value of $k_{obs} = 1.77 \times 10^{-12}$ cm^3 molecule^{-1} s^{-1} at 60 Torr and low CH_3OH concentration,[1] the value of ($\sigma_{HO_2} \times L$) is found from the analysis of decay curves to be 6.16×10^{-18} cm^3 at 296 K and 60 Torr. Since σ_{HO_2} is equal to 1.45×10^{-19} cm^2/molecule, L is equal to 42.5 cm, which is very close to what is obtained from a visual inspection of the cell and geometry of the laser beams. The deviation of ($\sigma_{HO_2} \times L$) measurements is <5%; therefore, the total experimental uncertainty of L is approximately 20%. It should be noted that to find the rate constants k_{obs} under different conditions, we used ($\sigma_{HO_2} \times L$), which is known with better precision than either σ_{HO_2} or L independently.

3. Measurements of k and k'' at 30 Torr as a Function of Temperature. From the measured HO_2 decays at 296 K and 30 Torr, and using the literature value for k, we find ($\sigma_{HO_2} \times L$) to be equal to 7.82×10^{-18} cm^3, giving $\sigma_{HO_2} = (1.84 \pm 0.36) \times 10^{-19}$ cm^2/molecule. As noted in subsection 2, σ_{HO_2} is found to be constant over the temperature range that we employed

TABLE 1: Temperature Dependence of the HO_2 Decay Rate Constant at Zero CH_3OH Concentration (k) and CH_3OH Enhancement Coefficient (k') at a Total Pressure of 30 Torr[a]

T (K)	k (cm^3 molecule^{-1} s^{-1})	k' (cm^6 molecule^{-2} s^{-1})	range of [CH_3OH] (10^{16} molecules cm^{-3})
253	$(2.37 \pm 0.06) \times 10^{-12}$	$(1.57 \pm 0.08) \times 10^{-28}$	0.1−1.2
263	$(2.21 \pm 0.05) \times 10^{-12}$	$(8.84 \pm 0.48) \times 10^{-29}$	0.1−1.6
273	$(1.94 \pm 0.02) \times 10^{-12}$	$(5.08 \pm 0.20) \times 10^{-29}$	0.1−2.0
283	$(1.83 \pm 0.03) \times 10^{-12}$	$(3.12 \pm 0.13) \times 10^{-29}$	0.2−3.4
296	$(1.71 \pm 0.02) \times 10^{-12}$	$(1.99 \pm 0.07) \times 10^{-29}$	0.4−5.6
311	$(1.63 \pm 0.01) \times 10^{-12}$	$(7.78 \pm 0.33) \times 10^{-30}$	1.1−6.1
323	$(1.55 \pm 0.03) \times 10^{-12}$	$(6.22 \pm 0.79) \times 10^{-30}$	1.1−5.9

[a] Errors quoted are $1-\sigma$ experimental uncertainty only.

(253−323 K). We then measured HO_2 decays as a function of CH_3OH concentration at different temperatures. The typical $[HO_2]_0$ was in the range of $\sim 1.7 \times 10^{13}$ to 3.6×10^{13} molecule/cm^3. Figure 3 shows the observed HO_2 decay rate constant versus [CH_3OH] at 273 and 311 K. It is apparent that the HO_2 decay rate constant increases with the increasing CH_3OH concentrations, with the magnitude of the effect increasing with decreasing temperature.

It is well-known that the presence of CH_3OH, the precursor of HO_2 radicals, can enhance the rate constant of HO_2 self-reaction. The overall mechanism[18,19] can be described as

$$HO_2 + HO_2 \rightarrow O_2 + H_2O_2 \quad (1)$$

$$HO_2 + HO_2 + M \rightarrow O_2 + H_2O_2 + M \quad (2)$$

$$HO_2 + CH_3OH \rightarrow HO_2 \cdot CH_3OH \quad (16)$$

$$HO_2 \cdot CH_3OH \rightarrow HO_2 + CH_3OH \quad (-16)$$

$$HO_2 + HO_2 \cdot CH_3OH \rightarrow \text{products} \quad (17)$$

$$HO_2 \cdot CH_3OH + HO_2 \cdot CH_3OH \rightarrow \text{products} \quad (18)$$

Using this scheme, the overall rate constant of HO_2 decay is equal to

$$k_{obs} = \frac{k + k_{17}K_C[CH_3OH] + k_{18}K_C^2[CH_3OH]^2}{1 + K_C[CH_3OH]} \quad (19)$$

where k_{obs} is the observed total HO_2 decay rate constant, k is the HO_2 decay rate constant at zero CH_3OH concentration, k_{17} is rate constant of reaction 17, k_{18} is rate constant of reaction 18, and K_C is the ratio of the rate constants of reactions 16 and –16. Note that for experiments using UV absorption for the detection of HO_2, the denominator of eq 19 should be squared. The maximum K_C[CH_3OH] used in this work was estimated to be approximately 0.32 on the basis of the equilibrium constants reported by Christensen et al.[18] The dependence of k_{obs} on [CH_3OH] was found to be linear and can be represented as

$$k_{obs} = k + k'[CH_3OH] \quad (20)$$

where k' is the CH_3OH enhancement coefficient on the rate constant of HO_2 self-reaction. Fitting the measurements shown in Figure 3 by using eq 20 provides the values of k and k'. Table 1 shows the results obtained at different temperatures. Both k and k' decrease with increasing temperature and have a negative activation energy. It should be noted that when the initial [Cl] was varied by a factor of 2, k_{obs} did not change noticeably. This suggests that the decay is second-order and that diffusion out of the photolysis volume is not a problem under our experimental conditions.

The source reaction for HO_2 also produces HCHO (see eq 8), which is known to react with HO_2 ($k \sim 4 \times 10^{-14}$ cm^3 molecule^{-1} s^{-1}).[1,11] The reaction is reversible but becomes irreversible at low temperatures as the reverse reaction slows down. The residence time in the cell was varied from 5.2 to 104 s in order to examine whether HCHO buildup was affecting the rate constant. If HCHO remained in the photolysis volume, an enhancement in the rate constant might have been expected. No change in k_{obs} was observed, implying that any HCHO produced was mixing into the full cross section of the cell and did not significantly affect the rate constant determination. A further set of experiments was carried out using C_2H_5OH in place of CH_3OH as the HO_2 source. The corresponding product, CH_3CHO, enhanced k_{obs} much less than HCHO. In these experiments, the values of k obtained at [C_2H_5OH] = 0 were identical to those using CH_3OH, again suggesting that HCHO production did not enhance the rate constants measured using CH_3OH as the HO_2 source.

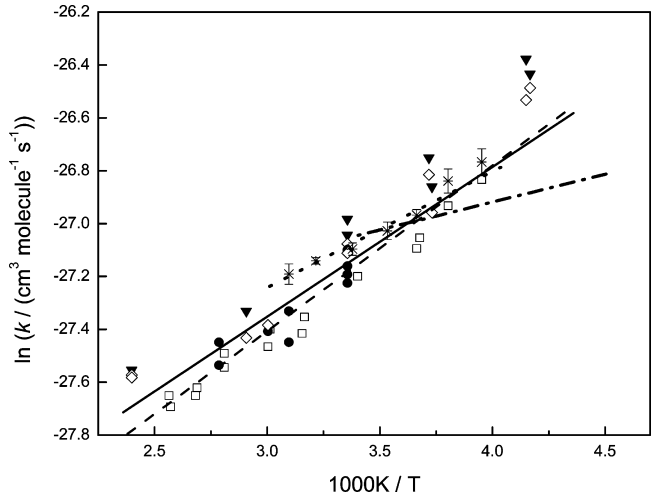

Figure 4. Comparison of the rate constants of the HO_2 self-reaction (k) from this work (asterisks with error bars) and from the literature, from Takacs and Howard[20] (open squares), from Thrush and Tyndall[21] (solid circles), and from Kircher and Sander[3] (solid triangles for those at 80−100 Torr of Ar or N_2 and open diamonds for those extrapolated to zero pressure). The dash−dot line represents the expression given by Christensen et al. (100 Torr, 222−295 K).[6] The dotted straight line is a weighted fit of our measurements. The dashed line is an unweighted fit of our measurements along with those from Takacs and Howard[20] and from Thrush and Tyndall;[21] the solid line is our recommended fit, based upon a normalization of the same data sets to a value of 1.65×10^{-12} cm^3 molecule^{-1} at 296 K.

Figure 4 shows our HO_2 self-reaction rate constants at zero [CH_3OH] along with the literature values. The values from this work are very close to those from Takacs and Howard[20] at low pressure (0−6 Torr), from Thrush and Tyndall[21] at 6−12 Torr, and from Kircher and Sander[3] at 100 Torr and extrapolated to zero pressure. Our work was conducted at 30 Torr; therefore, it is reasonable to compare our measurements to all of the above studies because the HO_2 decay rate constant only increases by

10% between 0 and 100 Torr. The corresponding expressions for the rate constant from these three references are

$$k = 2.0 \times 10^{-13} \times \exp(595/T) \quad (21)$$

$$k = 2.4 \times 10^{-13} \times \exp(560/T) \quad (22)$$

$$k = k_1 + k_2 = 2.2 \times 10^{-13} \times \exp(620/T) + 1.9 \times 10^{-33} \times [\mathrm{M}] \times \exp(980/T) \quad (23)$$

respectively. A weighted linear least-squares fit to our measurements, the solid line as shown in Figure 4, gives

$$k = (3.95 \pm 0.25) \times 10^{-13} \times \exp[(439 \pm 39)/T] \quad (24)$$

Here, the error quoted is the 1-σ deviation of the linear fit only. The activation energy shown in eq 24 is a little smaller than that from previous studies.

In contrast, the data of Christensen et al.[6] are quite different from those of previous studies. They accounted for the CH_3OH enhancement on the total observed decay rate constants the same way that we did. However, they reported a small activation energy and rate constants which are much lower than previous measurements at low temperature. The dash−dot line shown in Figure 4 represents the equation that they reported at 100 Torr

$$k = 8.8 \times 10^{-13} \times \exp(210/T) \quad (4)$$

It should be noted that Christensen et al. did not measure the rate constants at high temperature, that is, under conditions where the measured data would not be affected by CH_3OH because the complexation effect is weak. It seems unlikely that there is an inflection point near 296 K, which is implied from the rate constants at low temperature from Christensen et al. and those at high temperature from other groups. Since we do not know why the Christensen et al. data exhibit a different temperature dependence, we have not included them in the subsequent analysis.

A fit to our results combined with those from Takacs and Howard[20] and those from Thrush and Tyndall[21] gives $k = (1.91 \pm 0.18) \times 10^{-13} \times \exp[(627 \pm 30)/T]$ cm^3 molecule^{-1} s^{-1}, which is shown as the dashed line in Figure 4. The error quoted here is the deviation of the linear fit only. The data from Kircher and Sander were not included in the fit since it is not known how much they are influenced by methanol and formaldehyde at low temperature.

A more meaningful way to assess the temperature coefficient of k is to normalize the data to a common value near room temperature. In addition to the above studies, determinations of k have been made at low pressure near ambient temperature by Simonaitis and Heicklen,[22] Sander,[23] Rozenshtein et al.,[24] and Kurylo et al.[25] Adopting a value of 1.65×10^{-13} cm^3 molecule^{-1} s^{-1} at 296 K, the mean of all of the above low-pressure determinations, leads to the recommended expression (0−30 Torr) shown as the solid line in Figure 4

$$k = (2.45 \pm 0.50) \times 10^{-13} \times \exp[(565 \pm 130)/T] \quad (25)$$

The error bar in the A factor is the 95% uncertainty on the room-temperature determinations, while the uncertainty in the activation temperature is set to encompass the measurements used in the fit. It should be noted that the studies of Takacs and Howard,[20] Thrush and Tyndall,[21] and Rozenshtein et al.[24] all used independent calibration methods, while the others were all tied to UV absorption cross sections. The reported cross sections of Simonaitis and Heicklen[22] and Kurylo et al.[25] are all close to the currently recommended values,[11] while those used by Kircher and Sander[3] are roughly 10% higher.

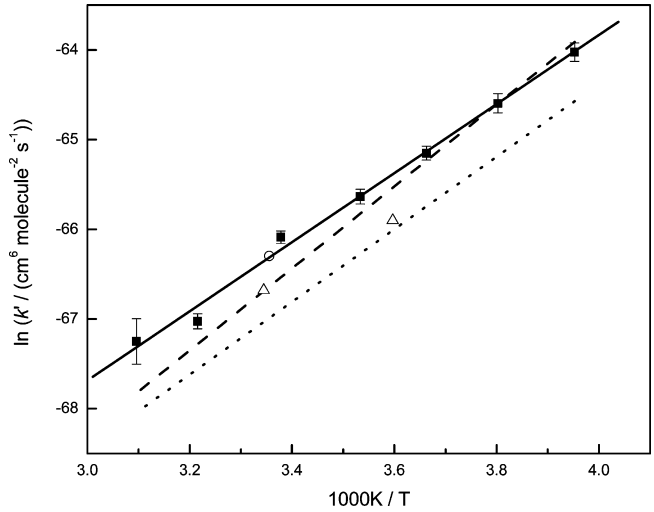

Figure 5. Arrhenius plot of the CH_3OH enhancement coefficient (k'). The solid squares are our measurements, and the solid line is the linear least-squares fit. The open circle is an estimation based on the report from Bloss et al.,[26] the open triangles are from Andersson et al.,[27] the dashed line is from Christensen et al.,[6] and the dotted line is from Stone and Rowley.[19]

Figure 5 shows the Arrhenius plot of our results for the CH_3OH enhancement coefficients (k'), which can be expressed as (uncertainties 1-σ precision)

$$k' = (3.90 \pm 1.87) \times 10^{-35} \times \exp[(3849 \pm 135)/T] \quad (26)$$

The open circle as shown in Figure 5 is an estimate from the work of Bloss et al.,[26] which was measured at 760 Torr O_2. The open triangles are the data reported by Andersson et al.[27] at 278 and 299 K in 760 Torr N_2. The dashed line is from Christensen et al.[6,18] at 100 Torr. They did not measure k' at high temperature, and the values quoted here were extrapolated from the pre-exponential factor (2.5×10^{-36} cm^6 molecule^{-2} s^{-1}) and activation energy (−38 kJ mol^{-1}) reported by Christensen et al. The dotted line is from the report of Stone and Rowley at 760 Torr,[19] $k' = 1.01 \times 10^{-35} \times \exp(4050/T)$ cm^6 molecule^{-2} s^{-1}.

While the values of k' are of similar magnitude, it should be noted that they may not be directly comparable since the total pressures are different. Kircher and Sander[3] found that the fractional enhancement by water vapor was the same at 100 and 700 Torr. The observation of Kircher and Sander requires that k_{17} and k_{18} have the same pressure dependence as k, which is hard to rationalize on a theoretical basis. However, our absolute enhancement by CH_3OH at 30 Torr is larger than that measured at 760 Torr (implying a much larger fractional enhancement). A systematic study of the methanol enhancement as a function of total pressure may lead to a better understanding of the overall reaction mechanism.

Measurements of the rate constant made using IR and UV do not have the same functional dependence on methanol. For UV data, where it is assumed that HO_2 and the complex are detected with equal sensitivity,[19] the denominator in eq 19 must be squared. Hence, the use of IR (where only uncomplexed HO_2 is detected) and UV gives rise to different slopes and intrinsically different enhancement factors. It is found empirically that k_{obs} depends linearly on the methanol concentration, even for

relatively large values of $K_C[CH_3OH]$. It is often stated that a linear dependence of k_{obs} on $[CH_3OH]$ will be found only if both $K_C[CH_3OH] \ll 1$ and $k_{18}K_C[CH_3OH] \ll k_{17}$. However, if $k_{18}K_C[CH_3OH]$ were very small, the observed rate constant would be observed to pass through a maximum and to decrease again at larger values of $K_C[CH_3OH]$, as observed in extreme cases for NH_3 addition by Hamilton and Lii.[5] In practice, the existence of linear plots suggests that $k_{18} \sim 2k_{17}$. Even though linear plots of k_{obs} versus $[CH_3OH]$ may be found using both IR and UV detection, the slopes should be different because of the different functionality related to the term in the denominator of eq 19.

Stone and Rowley[19] used methanol concentrations up to 4.5×10^{17} molecule/cm^3. Using the estimated values of k_{17} and K_C given by Christensen et al.,[18] considerable curvature should have been observed in Figure 6 of Stone and Rowley, k_{obs} versus $[CH_3OH]$. The values of k obtained by Stone and Rowley at low temperatures appear somewhat larger than those extrapolated from the current recommendations.[1,2,11] This could arise from fitting the data in their Figure 6 as a linear function rather than a curved one. If one forces their data at $[CH_3OH] = 0$ to match other studies, the experimental data can be fit adequately by the full expression for the rate constant as a function of $[CH_3OH]$, using the parameters given by Christensen et al.[18]

It should be noted that the values of k and k' reported here are based on an assumed rate constant, $k = 1.77 \times 10^{-12}$ cm^3 molecule^{-1} s^{-1} at 60 Torr total pressure and low CH_3OH concentration. Furthermore, they are based on the assumption that the CH_3OH enhancement effect on the rate constant of HO_2 decay can be ignored at low $[CH_3OH]$ and at 298 K, as mentioned in subsection 2. The value of k' that we found (1.73×10^{-29} cm^6 molecule^{-2} s^{-1} at 296 K) is 36% higher than that reported by Christensen and co-workers (1.27×10^{-29} cm^6 molecule^{-2} s^{-1} at 296 K).[6,18] Nonetheless, the corresponding contribution of CH_3OH enhancement to the total HO_2 decay rate constant is less than 2% at a CH_3OH concentration of 2.0×10^{15} molecule/cm^3, and hence, the approximation introduced above is completely acceptable. Varying the initial value of k that we used at 296 K and low CH_3OH concentration would only affect the pre-exponential factor shown in eq 24 but would not change the activation energy.

4. HO_2 Line Center Absorption Cross Sections as a Function of Pressure, Temperature, and Wavelength. Line center IR absorption cross sections were derived for HO_2 at different total pressures, temperatures, and wavelengths based on the measured rate constants. To do this, eqs 24 and 26 were used to calculate the HO_2 reaction rate constants as a function of $[CH_3OH]$. We also used the second term in eq 3 to correct k if the pressure was other than 30 Torr. For the CH_3OH enhancement coefficient (k') at other pressures, eq 26 was used without any other correction since k' is not expected to vary strongly over the pressure range studied. The effective absorption cross sections thus derived for the peak near 1506.43 nm are shown as the open squares in Figure 6. The effect of pressure broadening on the measured absorption cross section is clearly evident in the data. Only peak heights were used in this analysis, not full line shapes. Since the experiments were mainly designed to measure the kinetic decays of HO_2 radicals, insufficient points were taken on each scan to be able to determine the line shape with any precision. However, using peak heights leads to a less accurate determination of pressure broadening coefficients than if the full line shapes were used.

The dependence of the peak absorption cross sections on buffer gas can be represented by an empirical biexponential

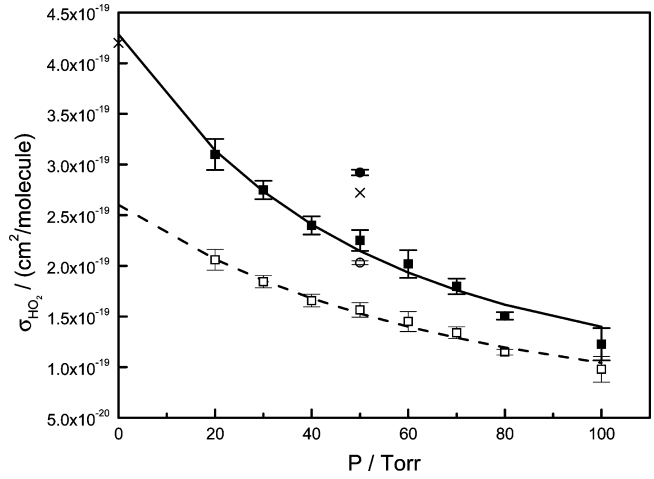

Figure 6. HO_2 absorption cross section as a function of the total pressure at 1506.43 nm and at 296 K. The open squares were measured in N_2 and O_2 (air), and the dashed line is a biexponential decay fit using eq 30. The open circle was measured in 76% He. The error bars quoted are experimental uncertainty only. The solid squares, solid circle, and solid line are the corresponding results after being corrected for the instrumental broadening effect. Also shown are the absorption cross section of HO_2 in 50 Torr of He and the Doppler absorption cross section of HO_2 (×) reported by Thiebaud et al.[13]

expression based on calculated Voigt profiles,[28] which is parametrized in terms of a normalized pressure broadening term, y.

$$\frac{\sigma}{\sigma_D} = 0.03044 + 0.3603\exp(-0.2969y) + 0.6032\exp(-1.560y) \quad (27)$$

Here, σ is the peak absorption cross section of the species studied and σ_D is its Doppler absorption cross section at zero pressure, and the expression should be general for all gases. The normalized pressure broadening term, y, is given by

$$y = \frac{\gamma_L}{\gamma_D}\sqrt{\ln 2} \quad (28)$$

where γ_L is the Lorentz width (HWHM) which includes all of the broadening effects (self-broadening and foreign broadening), that is, $\sum \gamma_M[M]$. γ_D is the Doppler width (HWHM) in cm^{-1} derived from

$$\gamma_D = 3.581 \times 10^{-7} \times \sqrt{\frac{T}{M}} \times \nu_0 \quad (29)$$

where T is the temperature (Kelvin), M is the molecular weight (atomic mass unit) and ν_0 is the center absorption frequency (cm^{-1}). In the present work, near-IR absorptions of C_2H_2 and N_2O were used to calibrate the instrument response. The Doppler widths of these two molecules bracket that of HO_2, and their IR absorption cross sections and buffer gas broadening coefficients have been well studied;[29] therefore, the molecules were good surrogates for HO_2. The experimentally measured peak heights could be well described by

$$\frac{\sigma}{\sigma_D} = 0.1132 + 0.2836\exp(-0.3403y) + 0.6032\exp(-1.560y) \quad (30)$$

which agrees with eq 27 within 10%, up to 120 Torr. Fitting our measurements shown in Figure 6 to eq 30 gives $\sigma_D = (2.6 \pm 0.2) \times 10^{-19}$ cm^2/molecule and $\gamma_{air} = (0.076 \pm 0.012)$ cm^{-1}/atm (HWHM). By comparing measurements of C_2H_2 and N_2O

lines with and without the 3 kHz filter, it was found that the filter introduced instrumental broadening, and thus, these are not the true values. Our HO_2 measurements were corrected to remove this effect by comparing the absorption intensities of C_2H_2 and N_2O with and without the filter. The correction factors at 20 and 100 Torr are 1.51 and 1.25, respectively. The corrected measurements are shown in Figure 6. Fitting these corrected measurements to eq 30 gives $\sigma_D = (4.3 \pm 1.1) \times 10^{-19}$ cm^2/molecule and $\gamma_{air} = (0.106 \pm 0.026)$ cm^{-1}/atm (HWHM), where the uncertainties represent 95% confidence limits, including all calibration factors discussed earlier.

If the cross sections were fit to eq 27, σ_D and γ_{air} would change by 1 and 8%, respectively. Our value of the air broadening coefficient γ_{air} is very close to that of several previous studies. Ibrahim and coauthors[30] reported that the average value for the lines with the lower state rotational quantum number $N'' = 3-10$ is approximately 0.115 cm^{-1}/atm. Nelson et al.[31] found $\gamma_{air} = (0.107 \pm 0.009)$ cm^{-1}/atm for the lines $N'' = 8$, and Kanno et al.[32] gave $\gamma_{air} = (0.101 \pm 0.013)$ cm^{-1}/atm for the lines $N'' = 16$. It should be mentioned that the relative concentration of O_2 varied in our experiments in order to maintain the efficiency of HO_2 production. Typically, it was 18−27%, which is very close to that in air, but in some extreme cases, it varied between 7 and 98%. No obvious dependence of the HO_2 absorption cross section on oxygen concentration was observed in this work.

Thiebaud et al.[13] found $\sigma_D = 4.2 \times 10^{-19}$ cm^2/molecule for the 1506.43 nm absorption feature, based on their measurements in 50 Torr of He, a result that is very close to ours. Helium usually has a more moderate collision efficiency than O_2 and N_2. We checked the HO_2 absorption cross section at the total pressure of 50 Torr, containing 76% He, 14% O_2, and 10% N_2, and found $\sigma_{HO_2} = 2.92 \times 10^{-19}$ cm^2/molecule, as shown in Figure 6, which is 30% larger than that in 50 Torr of N_2 and O_2 (2.25×10^{-19} cm^2/molecule). On the other hand, 2.92×10^{-19} cm^2/molecule is approximately equal to the HO_2 absorption cross section in 25 Torr of N_2 and O_2. Therefore, the He broadening coefficient is approximately one-third of the air broadening coefficient, which gives $\gamma_{He} = 0.035$ cm^{-1}/atm for this particular HO_2 absorption line. Thiebaud et al. measured a helium broadening coefficient of 0.057 cm^{-1}/atm for a different line in the same band, and our inferred value is close to that.

It should be pointed out that the rate constant (k) of HO_2 decay and the corresponding CH_3OH enhancement coefficient (k') discussed above will not change even though the absorption cross section needs correcting for the filter. Since the kinetic decays and the HO_2 cross section measurements relative to C_2H_2 were both taken using the 3 kHz filter, the broadened cross sections are appropriate for the kinetic analysis.

Besides 1506.43 nm, we also examined the weaker HO_2 absorptions at 1509.00 and 1509.26 nm for comparisons to other studies. The results at 30 Torr are presented in Table 2 along with several literature values.[13,14,33,34] The measurements of Thiebaud et al.[13] and Taatjes and OH[33] were both derived from a knowledge of the rate constant for $HO_2 + HO_2$ and the geometric path length of the absorption cell, while the measurements of Johnson et al.[14] were based on an absolute calibration in a flowing photolysis experiment. At room temperature, our result for the HO_2 absorption cross section at 1509.00 nm is 16% smaller than that from Thiebaud et al.,[13] while at 1509.26 nm, it is 17% larger than that from the Thiebaud study. One possible cause of this effect is that the air and He broadening coefficients might be different for different HO_2 absorption lines. There appears to be a shift of about 0.3 nm in the reported wavelengths of Johnson et al.[14] The corresponding wavelengths for peaks 14, 15, and 16 quoted from the Johnson et al. paper have been corrected in Table 2. If their data corresponded to 60 Torr of O_2, the absorption cross sections are in reasonable agreement with ours. In 100 Torr of N_2 and O_2, we found $\sigma_{HO_2} = 1.23 \times 10^{-19}$ cm^2/molecule at 1506.43 nm, as shown in Figure 6. This value is three times larger than the value quoted by Christensen et al., 4×10^{-20} cm^2/molecule at 100 Torr N_2/O_2,[34] which was based on an assessment of the previous literature.

TABLE 2: HO_2 Absorption Cross Sections at Different Wavelengths and Temperatures[a]

		σ (10^{-20} cm^2/molecule)				
T (K)	λ (nm)	this work	Thiebaud[b]	Johnson[c]	Taatjes[d]	Christensen[e]
~296	1506.43	27.5 ± 0.9	27.2			4
	1509.00	10.0 ± 1.1	11.9	5.3		
	1509.26	19.7 ± 1.1	16.8	10.4	10	
273	1506.43	27.5 ± 0.9				
	1509.00	10.1 ± 1.2				
	1509.26	18.8 ± 0.5				

[a] Our measurements were conducted at 30 Torr (mainly N_2 and O_2) and have been corrected for instrumental effects. [b] Reference 13. Measured in 50 Torr of He. [c] Reference 14. Reported as Doppler-limited but in 60 Torr of air (J. P. Burrows, personal communication, 2009). [d] Reference 33. Measured in 50 Torr of Ar. [e] Reference 34. Measured in 100 Torr of N_2/O_2.

When the temperature was decreased from 296 to 273 K, the HO_2 absorption cross section changed by 1% at 1509.00 nm and by 5% at 1509.26 nm, as shown in Table 2. Within the experimental uncertainties, no obvious temperature dependence on the HO_2 absorption cross sections was observed, which agrees with measurements of the stronger 1506.43 absorption line. The Doppler width of the lines should increase by about 10% over the full temperature range of the experiments (253−323 K). On the other hand, the pressure broadening coefficients typically show a $T^{-0.5}$ dependence (i.e., greater broadening at low temperature).[29] Since we are working in the intermediate pressure range between Doppler-limited and fully broadened, it is difficult to predict the extent, or even the sign, of the temperature coefficient. A small temperature dependence might also be masked by the instrumental broadening. Finally, we note that if we use eq 4 from Christensen et al. instead of eq 25 to calculate the HO_2 decay rate constant, the resulting HO_2 absorption cross sections decrease with the decreasing temperature, a ~12% change for a temperature change of only 23 K, a result that is larger than the expected trend.

5. Rate Constant Enhancement and Line Broadening by H_2O. The mechanism of the water vapor enhancement effect on the rate constant of HO_2 self-reaction is very similar to that of CH_3OH and can be described as

$$HO_2 + HO_2 \rightarrow O_2 + H_2O_2 \quad (1)$$

$$HO_2 + HO_2 + M \rightarrow O_2 + H_2O_2 + M \quad (2)$$

$$HO_2 + H_2O \rightarrow HO_2 \cdot H_2O \quad (31)$$

$$HO_2 \cdot H_2O \rightarrow HO_2 + H_2O \quad (-31)$$

$$HO_2 + HO_2 \cdot H_2O \rightarrow \text{products} \quad (32)$$

$$HO_2 \cdot H_2O + HO_2 \cdot H_2O \rightarrow \text{products} \quad (33)$$

By using this scheme, the overall rate constant of HO_2 decay is represented by

$$k_{obs} = k + k''[H_2O] \quad (34)$$

where k'' is the H_2O enhancement coefficient on the rate constant of HO_2 self-reaction. For these determinations, the concentration

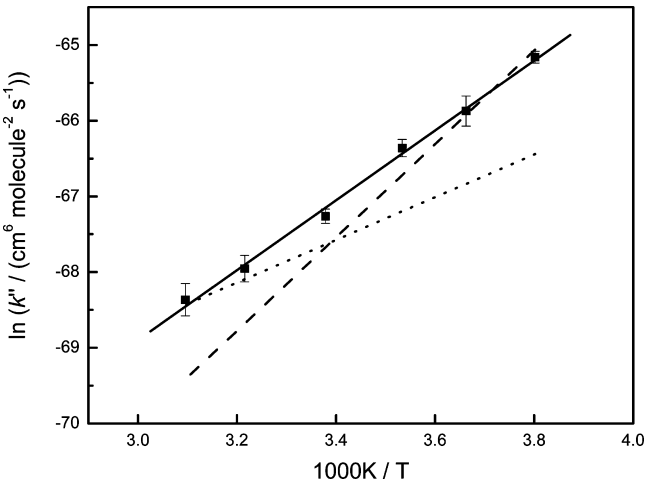

Figure 7. Arrhenius plot of the water vapor enhancement coefficient (k'') on the HO_2 decay rate. The solid squares are our measurements, and the solid line is the linear least-squares fit. The dashed line is based on the equation from Stone and Rowley,[19] and the dotted line is from Kircher and Sander.[3]

and enhancement effect of CH_3OH was minimized and included in the value of k.

The absolute concentration of water vapor in the cell was measured by using IR absorption at ~1508.28 nm, referring to the absolute line strength from the HITRAN database.[29] The concentration was also estimated by UV absorption at 184.9 nm in a 25 cm cell,[35] which was positioned upstream of the Herriott cell. At the concentrations of H_2O used, it was necessary to account for broadening of the water vapor absorption lines by both N_2 and itself based on eq 30. Pressure-broadened H_2O absorption cross sections were measured in both static and flowing mixtures.

Water vapor not only complexes with HO_2 radicals but also broadens HO_2 near-IR absorption peaks.[32] For the HO_2 absorption line that we observed, the water vapor broadening coefficient was found to be approximately 4.1 times larger than air. We used $\gamma_{air} = 0.106$ cm^{-1}/atm and $\gamma_{H_2O} = 0.435$ cm^{-1}/atm at room temperature, with both values changing only slightly with temperature.

After accounting for the water vapor broadening of the HO_2 absorption peak, the water vapor enhancement coefficient on the HO_2 self-reaction is derived and shown in Figure 7. The linear fit to the data gives

$$k'' = (1.16 \pm 0.58) \times 10^{-36} \times \exp[(4614 \pm 145)/T] \quad (35)$$

Two previous studies using UV absorption, from Kircher and Sander[3] (measured at 100 and 700 Torr) and Stone and Rowley[19] (measured between 400 and 760 Torr), are also shown in Figure 7. Again, direct comparison of the result is difficult as a result of the different pressure ranges used and the different techniques used (UV versus IR).

Conclusions

The spectroscopic and kinetic properties of HO_2 radicals were characterized by using diode laser absorption in the near-IR region. By using a literature value for k at 296 K and 30 Torr, we derived a temperature-dependent rate constant for the HO_2 self-reaction of $(3.95 \pm 0.45) \times 10^{-13} \times \exp[(439 \pm 39)/T]$ cm^3 molecule^{-1} s^{-1}, which exhibits an activation energy larger than that reported by Christensen et al.[6] Taking previous studies at low pressure into account, the rate constant of HO_2 self-reaction k that we recommend is $(2.45 \pm 0.50) \times 10^{-13} \times \exp[(565 \pm 130)/T]$ cm^3 molecule^{-1} s^{-1}. We also determined the CH_3OH enhancement coefficient, $k' = (3.90 \pm 1.87) \times 10^{-35} \times \exp[(3849 \pm 135)/T]$ cm^6 molecule^{-2} s^{-1}, and the water vapor enhancement coefficient, $k'' = (1.16 \pm 0.58) \times 10^{-36} \times \exp[(4614 \pm 145)/T]$ cm^6 molecule^{-2} s^{-1}, both at 30 Torr total pressure. Christensen et al. showed that stratospheric measurements of H_2O_2 could be modeled much better using their temperature dependence for $HO_2 + HO_2$ reactions. Our measurements show that the value of the rate constant in the stratosphere should be larger, which would lead to less HO_2 and more H_2O_2 in the models. The exact functional form of the rate constant remains uncertain, and it is suggested that new experiments be performed to systematically characterize the water vapor and methanol enhancements at high pressure.

The HO_2 absorption cross sections were examined at 1506.43, 1509.00, and 1509.26 nm. The strongest absorption at 1506.43 nm was also measured in the pressure range of 20−100 Torr, which gave the air broadening coefficient (0.106 ± 0.026) cm^{-1}/atm (HWHM) and the HO_2 absorption cross section at zero pressure $(4.3 \pm 1.1) \times 10^{-19}$ cm^2/molecule.

Acknowledgment. We thank P. Seakins for providing construction details of the Herriott cell and A. Fried, C. A. Taatjes, and S. P. Sander for discussions on the spectroscopy and kinetics of HO_2 radicals. We thank A. Fried, R. Hornbrook, and two anonymous reviews for their helpful comments on the manuscript. The National Center for Atmospheric Research is operated by the University Corporation for Atmospheric Research, under the sponsorship of the National Science Foundation. This work was supported by a grant from the NASA Upper Atmosphere Research Program (NNG06GE44G).

References and Notes

(1) Atkinson, R.; Baulch, D. L.; Cox, R. A.; Crowley, J. N.; Hampson, R. F.; Hynes, R. G.; Jenkin, M. E.; Rossi, M. J.; Troe, J. *Atmos. Chem. Phys.* **2004**, *4*, 1461–1738.

(2) Wallington, T. J.; Dagaut, P.; Kurylo, M. J. *Chem. Rev.* **1992**, *92*, 667–710.

(3) Kircher, C. C.; Sander, S. P. *J. Phys. Chem.* **1984**, *88*, 2082–2091.

(4) Hamilton, E. J., Jr. *J. Chem. Phys.* **1975**, *63*, 3682–3683.

(5) Hamilton, E. J., Jr.; Lii, R. R. *Int. J. Chem. Kinet.* **1977**, *9*, 875–885.

(6) Christensen, L. E.; Okumura, M.; Sander, S. P.; Salawitch, R. J.; Toon, G. C.; Sen, B.; Blavier, J.-F.; Jucks, K. W. *Geophys. Res. Lett.* **2002**, *29*, 1299.

(7) Suma, K.; Sumiyoshi, Y.; Endo, Y. *Science* **2006**, *311*, 1278–1281.

(8) English, A. M.; Hansen, J. C.; Szente, J. J.; Maricq, M. M. *J. Phys. Chem. A* **2008**, *112*, 9220–9228.

(9) Aloisio, S.; Francisco, J. S.; Friedl, R. R. *J. Phys. Chem. A* **2000**, *104*, 6597–6601.

(10) Cox, R. A.; Burrows, J. P. *J. Phys. Chem.* **1979**, *83*, 2560–2568.

(11) Sander, S. P.; Friedl, R. R.; Golden, D. M.; Kurylo, M. J.; Moortgat, G. K.; Keller-Rudek, H.; Wine, P. H.; Ravishankara, A. R.; Kolb, C. E.; Molina, M. J.; Finlayson-Pitts, B. J.; Huie, R. E.; Orkin, V. L. *Chemical Kinetics and Photochemical Data for Use in Atmospheric Studies*, Evaluation No. 15; Jet Propulsion Laboratory: Pasadena, CA, 2006; web address: http://jpldataeval.jpl.nasa.gov/pdf/JPL_15_AllInOne.pdf, http://jpldataeval.jpl.nasa.gov/pdf/Jpl15_Sectn1_BiomolecRxs.pdf.

(12) Thiebaud, J.; Fittschen, C. *Appl. Phys.* **2006**, *85*, 383–389.

(13) Thiebaud, J.; Crunaire, S.; Fittschen, C. *J. Phys. Chem. A* **2007**, *111*, 6959–6966.

(14) Johnson, T. J.; Wienhold, F. G.; Burrows, J. P.; Harris, G. H.; Burkhard, H. *J. Phys. Chem.* **1991**, *95*, 6499–6502.

(15) Pilgrim, J. S.; Jennings, R. T.; Taatjes, C. A. *Rev. Sci. Instrum.* **1997**, *68*, 1875–1878.

(16) Qian, H.; Turton, D.; Seakins, P. W.; Pilling, M. J. *Chem. Phys. Lett.* **2000**, *322*, 57–64.

(17) Braun, W.; Herron, J. T.; Kahaner, D. K. *Int. J. Chem. Kinet* **1988**, *20*, 51–62.

(18) Christensen, L. E.; Okumura, M.; Hansen, J. C.; Sander, S. P.; Francisco, J. S. *J. Phys. Chem. A* **2006**, *110*, 6948–6959.

(19) Stone, D.; Rowley, D. M. *Phys. Chem. Chem. Phys.* **2005**, *7*, 2156–2163.
(20) Takacs, G. A.; Howard, C. J. *J. Phys. Chem.* **1986**, *90*, 687–690.
(21) Thrush, B. A.; Tyndall, G. S. *Chem. Phys. Lett.* **1982**, *92*, 232–235.
(22) Simonaitis, R.; Heicklen, J. *J. Phys. Chem.* **1982**, *86*, 3416–3418.
(23) Sander, S. P. *J. Phys. Chem.* **1984**, *88*, 6018–6021.
(24) Rozenshtein, V. B.; Gershenzon, Y. M.; Il'in, S. D.; Kishkovitch, O. P. *Chem. Phys. Lett.* **1984**, *112*, 473–478.
(25) Kurylo, M. J.; Ouellette, P. A.; Laufer, A. H. *J. Phys. Chem.* **1986**, *90*, 437–440.
(26) Bloss, W. J.; Rowley, D. M.; Cox, R. A.; Jones, R. L. *Phys. Chem. Chem. Phys.* **2002**, *4*, 3639–3647.
(27) Andersson, B. Y.; Cox, R. A.; Jenkin, M. E. *Int. J. Chem. Kinet.* **1988**, *20*, 283–295.
(28) Fried, A.; Richter, D. In *Analytical Techniques for Atmospheric Measurement*; Heard, D. E., Ed.; Blackwell Publising: Oxford, U.K., 2006; p 92.
(29) Rothman, L. S.; Jacquemart, D.; Barbe, A.; Benner, D. C.; Birk, M.; Brown, L. R.; Carleer, M. R.; Chackerian, C., Jr.; Chance, K.; Coudert, L. H.; Dana, V.; Devi, V. M.; Flaud, J.-M.; Gamache, R. R.; Goldman, A.; Hartmann, J.-M.; Jucks, K. W.; Maki, A. G.; Mandin, J.-Y.; Massie, S. T.; Orphal, J.; Perrin, A.; Rinsland, C. P.; Smith, M. A. H.; Tennyson, J.; Tolchenov, R. N.; Toth, R. A.; Vander Auwera, J.; Varanasi, P.; Wagner, G. The HITRAN Database. http://www.cfa.harvard.edu/HITRAN/ (2009).
(30) Ibrahim, N.; Thiebaud, J.; Orphal, J.; Fittschen, C. *J. Mol. Spectrosc.* **2007**, *242*, 64–69.
(31) Nelson, D. D., Jr.; Zahniser, M. S. *J. Mol. Spectrosc.* **1994**, *166*, 273–279.
(32) Kanno, N.; Tonokura, K.; Tezaki, A.; Koshi, M. *J. Mol. Spectrosc.* **2005**, *229*, 193–197.
(33) Taatjes, C. A.; Oh, D. B. *Appl. Opt.* **1997**, *36*, 5817–5821.
(34) Christensen, L. E.; Okumura, M.; Sander, S. P.; Friedl, R. R.; Miller, C. E.; Sloan, J. J. *J. Phys. Chem. A* **2004**, *108*, 80–91.
(35) Cantrell, C. A.; Zimmer, A.; Tyndall, G. S. *Geophys. Res. Lett.* **1997**, *24*, 2195–2198.

JP905279B